



Cite this: *Phys. Chem. Chem. Phys.*,
2017, 19, 14048

Structure and dynamics of water confined in a graphene nanochannel under gigapascal high pressure: dependence of friction on pressure and confinement

Lei Yang,^a Yanjie Guo^a and Dongfeng Diao^{a,b*}

Recently, water flow confined in nanochannels has become an interesting topic due to its unique properties and potential applications in nanofluidic devices. The trapped water is predicted to experience high pressure in the gigapascal regime. Theoretical and experimental studies have reported various novel structures of the confined water under high pressure. However, the role of this high pressure on the dynamic properties of water has not been elucidated to date. In the present study, the structure evolution and interfacial friction behavior of water constrained in a graphene nanochannel were investigated via molecular dynamics simulations. Transitions of the confined water to different ice phases at room temperature were observed in the presence of lateral pressure at the gigapascal level. The friction coefficient at the water/graphene interface was found to be dependent on the lateral pressure and nanochannel height. Further theoretical analyses indicate that the pressure dependence of friction is related to the pressure-induced change in the structure of water and the confinement dependence results from the variation in the water/graphene interaction energy barrier. These findings provide a basic understanding of the dynamics of the nanoconfined water, which is crucial in both fundamental and applied science.

Received 28th March 2017,
Accepted 5th May 2017

DOI: 10.1039/c7cp01962a

rscl.li/pccp

1. Introduction

The recent development of nanotechnology has potentiated the fabrication of nanofluidic devices.^{1–3} Application of these devices requires an understanding of the fluid flows in nanoscopic spaces and interfaces. Water flow confined in nanopores or nanochannels has been an interesting topic over the last few years due to its unique properties in materials science, biology, tribology, and nanoscience. When water is confined in spaces of several nanometers, especially near the hydrophobic surfaces, the solid/liquid interfaces can induce unconventional behaviors of the water flow.^{4–8} Owing to its ultrathin and hydrophobic nature, graphene has emerged as one of the most promising materials for the construction of nanochannels for water flow. A number of studies have been reported on the exceptional structure and dynamics of water constrained in a graphene-derived nanochannel.^{9–14} However, water molecules were predicted to experience a pressure in the gigapascal

regime under this hydrophobic confinement. Nair *et al.* estimated the capillary pressure applied on the constrained water to be as high as 1 GPa.¹⁵ In the latest study of Vasu *et al.*, the van der Waals pressure on the trapped interlayer molecules was found to be 1.2 ± 0.3 GPa, measured *via* Raman spectroscopy.¹⁶ This high pressure would have substantial effects on the physical, chemical, and structural properties of interfacial water, which should be taken into account for the development of nanofluidic devices.

To date, a number of theoretical studies have been carried out to explore the structure evolution of the nanoconfined water in the presence of high pressure. These studies have predicted a number of novel structures for the confined water.^{17–19} From an experimental perspective, a recent transmission electron microscopy study of the water layers trapped between hydrophobic graphene walls has reported a phase transition of water from the liquid state to square ice at room temperature, and the pressure for confining water was estimated to be about 1 GPa.²⁰ Although extensive studies have been carried out on the structure change of water, the dynamics of water under these high pressures in the gigapascal regime have not been comprehensively explored. Friction is one of the most important dynamic properties that influence the flow behavior at the nanoscale.^{21,22} Basic understanding of the interfacial friction in a nanochannel is important both in fundamental and applied science.

^a Key Laboratory of Education Ministry for Modern Design and Rotor-Bearing System, School of Mechanical Engineering, Xi'an Jiaotong University, Xi'an 710049, China

^b Institute of Nanosurface Science and Engineering (INSE), Shenzhen University, Shenzhen 518060, China. E-mail: dfdiao@szu.edu.cn; Tel: +86-755-26902415

Previous studies have revealed that interfacial friction of water was affected by the surface curvature,^{2,3} atomic structure,²⁴ and mechanical strain²⁵ of the confining wall. As for the pressure effect, Falk *et al.* mentioned in their study that the friction coefficient of water between planar graphene sheets was independent of pressure below 500 atm (50 MPa).²³ However, the situation might be different when the pressure increases to gigapascal levels. Therefore, further understanding of the interfacial friction of water inside the nanochannel under gigapascal pressures is indispensable.

In this study, equilibrium molecular dynamics (MD) simulations of water constrained in a graphene-based nanochannel were performed. The pressure-induced structure evolution of the confined water at different nanochannel heights was investigated. The dependence of the interfacial friction coefficient on the lateral pressure and nanochannel height was explored. Further analyses were conducted to understand the physical origin of the dependence of friction on the lateral pressure and confinement.

2. Computational methods

A schematic of the model used in our simulation is illustrated in Fig. 1. The simulation system includes two parts: two water reservoirs at the two ends and the nanochannel built with a pair of trilayer graphene sheets. Each graphene layer was $50 \text{ \AA} \times 50 \text{ \AA}$ in size, containing 1008 carbon atoms. The height h of the nanochannel ranged from 6 to 10 \AA . Herein, two water reservoirs containing 600 molecules each were connected by the graphene nanochannel. The extended four-point charge model (TIP4P/2005) was used to construct the water molecules, including a long-range Coulomb potential and a short-range Lennard–Jones (LJ) potential.²⁶ The cut-off distance for the Coulomb interaction was 8.5 \AA and that for LJ interaction was 12.0 \AA . The interaction parameters of O–O, O–H, and H–H were determined to be $\sigma_{\text{O-O}} = 3.1589 \text{ \AA}$, $\epsilon_{\text{O-O}} = 0.1852 \text{ kcal mol}^{-1}$, $\sigma_{\text{O-H}} = 0$, $\epsilon_{\text{O-H}} = 0$, $\sigma_{\text{H-H}} = 0$, and $\epsilon_{\text{H-H}} = 0$,²⁷ where σ is related to the equilibrium atom distance and ϵ is the well depth of the potential. The water–graphene interaction was

described by the LJ potential between the oxygen atoms of water and the carbon atoms of graphene. The interaction parameters were found to be $\sigma_{\text{C-O}} = 3.19 \text{ \AA}$ and $\epsilon_{\text{C-O}} = 0.09369 \text{ kcal mol}^{-1}$, reported by Werder *et al.*²⁸ The Werder parameters were originally defined using the SPC/E water model. However, researchers also used these parameters for TIP4P,²⁹ TIP4P/2005,³⁰ and TIP5P³¹ to reproduce the water contact angle on the graphene surface. In addition, according to ref. 20, the results of SPC/E and TIP4P/2005 water constrained between graphene sheets were the same, obtained using the Werder parameters.

Equilibrium molecular dynamics simulations were performed using the large-scale atomic/molecular massively parallel simulator (LAMMPS) package.³² The Velocity-Verlet algorithm was used for integration with a time step of 1 fs. The long-range interactions were computed using the particle–particle particle–mesh (PPPM) algorithm. The SHAKE algorithm was used to constrain the angle and bond length of TIP4P/2005 water. The graphene wall was kept rigid during the simulation by fixing the positions of the carbon atoms. Periodic boundary conditions were applied along all three directions of the simulation box. All the simulations performed were based on the constant pressure and temperature (NPT) ensemble, where pressure and temperature were controlled by the Nosé–Hoover thermostat and barostat. Initially, the system was equilibrated for 5 ns at a temperature of 300 K and lateral pressure P (along the x -axis) of 0.1 GPa. After equilibration, P was increased by 0.2 GPa per 1 ns, whereas the temperature was kept at 300 K. For $h = 6, 6.5,$ and 7 \AA , the maximum lateral pressure was 3.1 GPa and the corresponding pressurization time was 15 ns. For $h = 8, 9,$ and 10 \AA , the maximum lateral pressure was 4.1 GPa and the corresponding pressurization time was 20 ns. After the pressurization process, water molecules were still left in the water reservoirs. The number of remaining water molecules depended on h and P . These remaining water molecules could enter the nanochannel *via* further increasing the confinement height or the lateral pressure. In all the simulations, the pressure along y and z axes was not controlled, and the box dimensions along these axes were kept fixed.

To evaluate the dynamics of the nanoconfined water, we calculated the friction coefficient λ at the water/graphene interface under the given P and h conditions. λ was defined as the ratio between the friction force parallel to the graphene wall per unit area and the slip velocity. It was obtained using the Green–Kubo (GK) relationship, which calculates the integration of the frictional force autocorrelation function in the equilibrium molecular dynamics simulations.³³

$$\lambda = \frac{1}{Ak_{\text{B}}T} \int_0^{\infty} dt \langle F(t)F(0) \rangle_{\text{equ}} \quad (1)$$

where A is the surface area of the graphene wall, k_{B} is the Boltzmann constant, T is the temperature, and $F(t)$ is the total tangential force acting along the x -axis at the liquid/solid interface. In our simulations, the force autocorrelation function was calculated every 2 fs for a duration of 0.5 ns. Herein, note that the cut-off time of the autocorrelation function integration was significant for the accuracy of the friction coefficient value. In this study, the cut-off time was chosen as the first zero of the

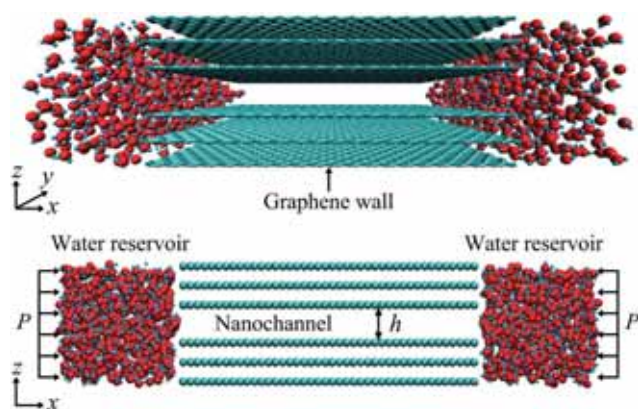


Fig. 1 Atomic configuration of the simulation model: water molecules confined in a graphene nanochannel with the height of h . The lateral pressure P was applied along the x -axis.

force autocorrelation function according to the work of Espanol *et al.*³⁴

3. Results and discussion

3.1 Structure evolution of the confined water

Fig. 2(a)–(c) show the area density of the confined water as a function of the lateral pressure P at $h = 6 \text{ \AA}$, 6.5 \AA , and 7 \AA . The area density is defined as the total number of water molecules per unit area. The inset figures show the typical images of the water structures under different pressures. As shown in the figure, the area density gradually increases with P . At $h = 6 \text{ \AA}$ and 6.5 \AA , the monolayer water transforms into a flat monolayer square-like ice (fMSI) when the lateral pressure is beyond 1.8 GPa with a critical area density around 13.0 nm^{-2} (Fig. 2(a) and (b)), which is consistent with the value reported in the work of Zhao *et al.*³⁵ For this fMSI, all the oxygen atoms are located in the same plane, arranged in square-like rings. In comparison, at $h = 7 \text{ \AA}$, a puckered monolayer square-like ice (pMSI) was formed when P increases to 2.4 GPa at the critical area density of around 15.2 nm^{-2} (Fig. 2(c)). In the pMSI structure, the oxygen atoms are also arranged in square-like rings. However, unlike fMSI, the oxygen atoms of pMSI are located at different heights along

the z -axis and the separation is not large enough to form two layers. Similar monolayer ice phases have been reported in previous works.^{18–20,35} To further determine the difference between fMSI and pMSI, the oxygen atom distribution profiles along the z -axis of fMSI and pMSI are presented in Fig. 2(d). It can be clearly observed that the profile of fMSI has only one peak, whereas that of pMSI shows two peaks, corresponding to different structures of these two types of monolayer ices.

Fig. 3(a)–(c) show the area density of confined water as a function of P at $h = 8 \text{ \AA}$, 9 \AA , and 10 \AA and the typical images of the water structures under different pressures. It can be observed that the initial structures of the confined water are bilayer liquid at these three confinement heights. At $h = 8 \text{ \AA}$, the area density increases with the lateral pressure until a transition from bilayer water to AB-stacked bilayer ice occurs. The critical pressure for this transition is 3.2 GPa, with an area density of 26.3 nm^{-2} (Fig. 3(a)). In the AB-stacked bilayer ice, water molecules are clearly located in two layers. Each layer has a rhombic lattice for the oxygen atoms, and there is a mismatching between oxygen atoms in the adjacent layers. However, the situation is different at $h = 9 \text{ \AA}$. In this case, AA-stacked bilayer ice is formed when P increases up to 1.8 GPa, with an area density of 26.4 nm^{-2} (Fig. 3(b)), almost equal to that of the AB-stacked structure. The in-plane oxygen atoms of the AA-stacked ice are

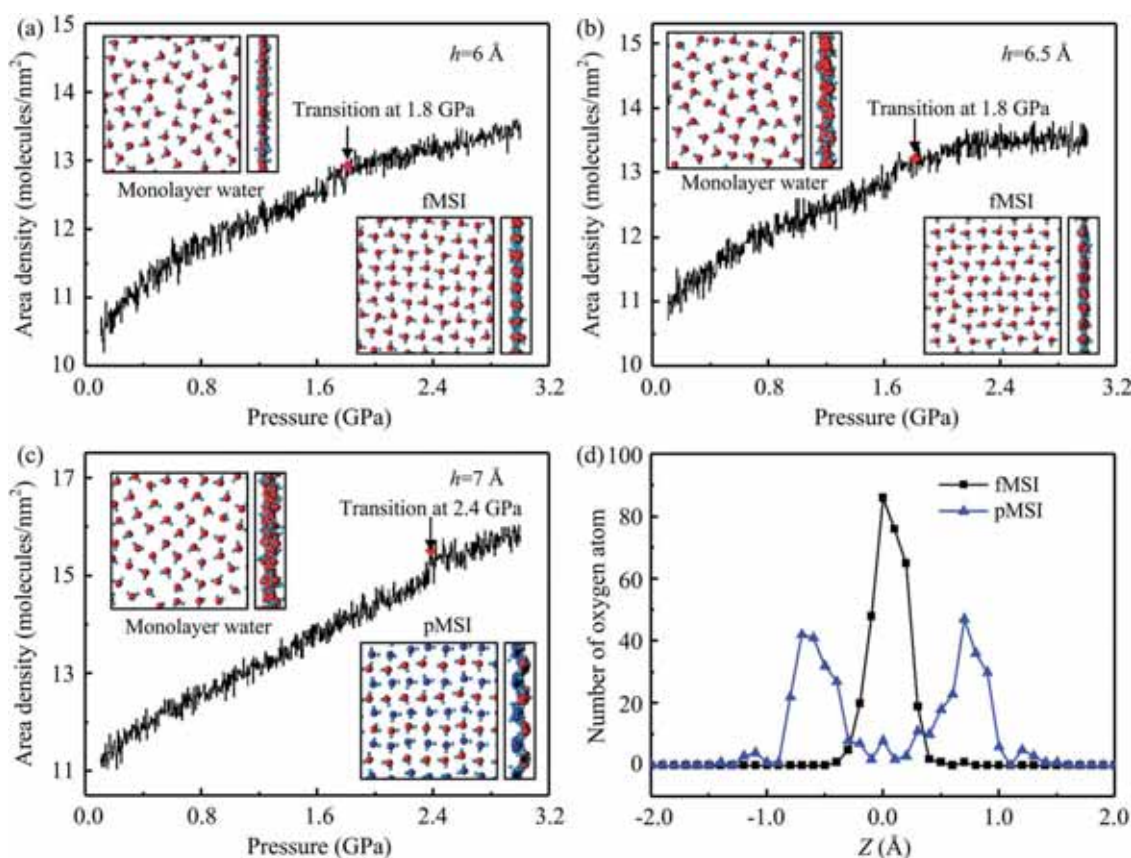


Fig. 2 (a–c) The pressure-induced area density variations and the corresponding structures of the water molecules constrained in nanochannels of height $h = 6 \text{ \AA}$, 6.5 \AA , and 7 \AA , respectively. The red and blue oxygen atoms denote different heights along the z -axis. (d) The oxygen atom distribution profiles along the z -axis of flat monolayer square-like ice (fMSI) and puckered monolayer square-like ice (pMSI).

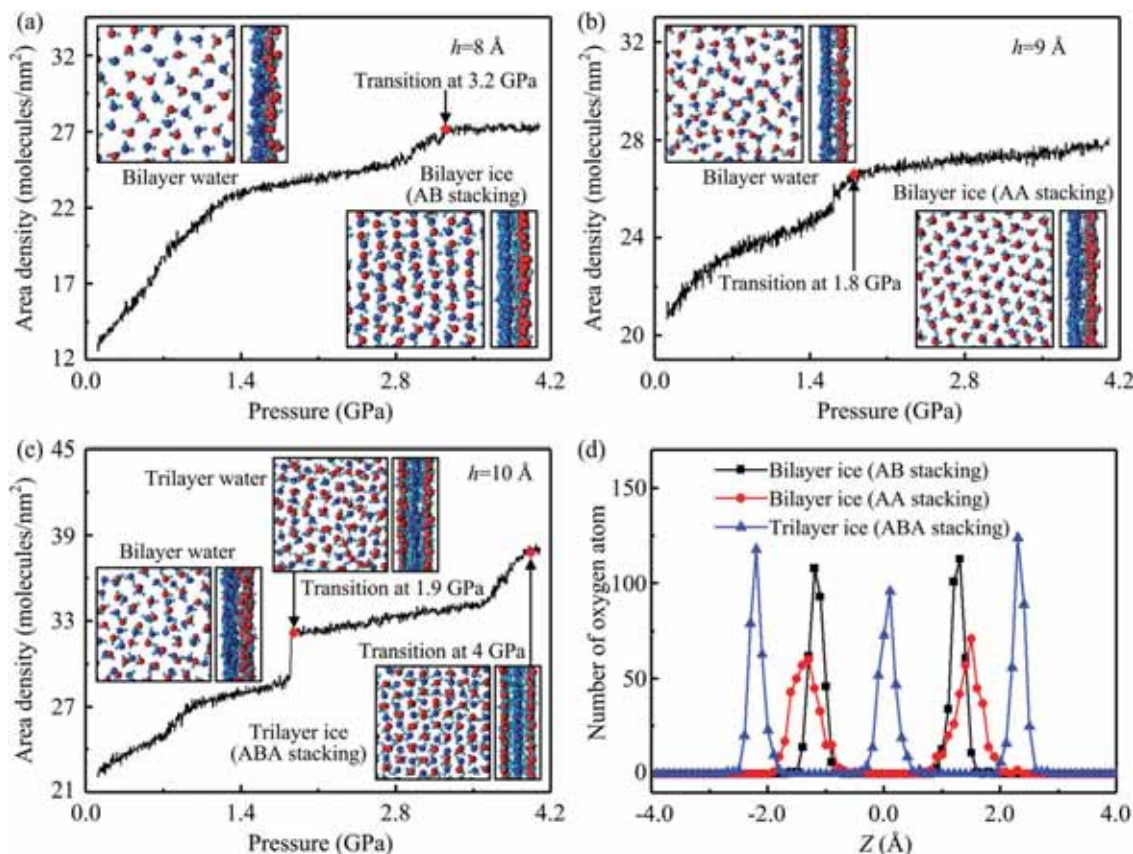


Fig. 3 (a–c) The pressure-induced area density variations and the corresponding phase transitions of water molecules constrained in nanochannels of height $h = 8$ Å, 9 Å, and 10 Å, respectively. The red and blue oxygen atoms denote different heights along the z -axis. (d) The oxygen atom distribution profiles along the z -axis of AB-stacked bilayer ice, AA-stacked bilayer ice, and ABA-stacked trilayer ice.

also arranged in rhombic rings, and the oxygen atoms in the adjacent layers are superimposed on top of one another, which is different from the AB-stacked structure. At $h = 10$ Å, two transitions occurred with the increasing P (Fig. 3(c)). The first transition from bilayer water to trilayer water appears at $P = 1.9$ GPa, leading to a sharp increase in the area density. Further increase of P to 4 GPa results in the second transition of the trilayer water to ABA-stacked trilayer ice, with an area density of 38.3 nm^{-2} . The abovementioned bilayer and trilayer ice structures are consistent with the previously reported structures.^{17,18} Fig. 3(d) depicts the oxygen atom distribution profiles along the z -axes of the two bilayer ices and the trilayer ice. The number of peaks in each profile is consistent with the layer number of the corresponding ice structure.

3.2 Pressure and nanochannel height-dependent friction coefficient

To explore the dynamics of the confined water under gigapascal pressure, the friction coefficients at the water/graphene interface under different P and h conditions were calculated. λ can be obtained from eqn (1), as mentioned in Section 2. Herein, note that eqn (1) is only suitable when the confined water is in liquid phase. Therefore, according to the abovementioned results, P was ~ 1 GPa for the calculation of the friction

coefficient when the confined water was still in the liquid phase. Fig. 4 summarizes the results for the friction coefficient of the monolayer water as a function of the lateral pressure at $h = 6$ Å, 6.5 Å, and 7 Å. It is apparent that the friction coefficient gradually increased with the increasing P . For bilayer water at $h = 8$ Å, 9 Å, and 10 Å, λ exhibits a similar trend with the

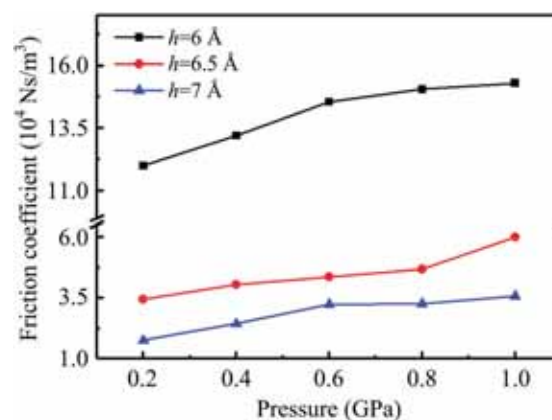


Fig. 4 Friction coefficient of the monolayer water at the water/graphene interface as a function of the lateral pressure at $h = 6$ Å, 6.5 Å, and 7 Å. The error bars are not shown since they are smaller than the symbol size.

increasing lateral pressure. This pressure-dependent friction of the confined water was quite interesting since the friction coefficient of the confined water inside the graphene nanochannel was found to be independent of pressure below 500 atm (50 MPa), as reported by Falk *et al.*²³ According to the work of Falk *et al.*, the interfacial friction coefficient was around $1.2 \times 10^4 \text{ N s m}^{-3}$ when $h \geq 6.8 \text{ \AA}$ and $P \leq 50 \text{ MPa}$. Herein, we also calculated the friction coefficient of the confined water under this low pressure regime using our model. For $h = 7 \text{ \AA}$, the interfacial friction coefficients under the pressures of 0.1 MPa, 1 MPa, and 10 MPa were $1.711 \times 10^4 \text{ N s m}^{-3}$, $1.707 \times 10^4 \text{ N s m}^{-3}$, and $1.735 \times 10^4 \text{ N s m}^{-3}$, respectively. Apparently, the friction coefficient is independent of pressure in this regime, consistent with the work of Falk *et al.* The different friction coefficient values obtained in these two studies under the low pressure regime could be caused by different water models and different C–O interaction parameters.

Another interesting point shown in Fig. 4 is that the friction coefficient declines as the height of the nanochannel increases under a constant pressure, indicating that the frictional behavior of the confined water also depends on the confinement height. To clarify this confinement effect on friction, the interfacial friction coefficients at different confinement heights were calculated under a fixed pressure. Fig. 5 illustrates the friction coefficient variation with h under $P = 0.4 \text{ GPa}$. Apparently, the friction coefficient is strongly dependent on the nanochannel height. When h is below 7 \AA , under which the confined water is a monolayer liquid, the friction coefficient decays with the nanochannel height. The abrupt increase of λ at 8 \AA is related to the formation of the bilayer water. For the bilayer water, the friction coefficient also shows a decreasing tendency with h . The reason for this dependence of λ on the lateral pressure and nanochannel height has been discussed in the following section.

3.3 Origin of the dependence of friction

To interpret the origin of the dependence of the interfacial friction coefficient on the lateral pressure and nanochannel height, an analytical theory proposed by Falk *et al.* was used.²³

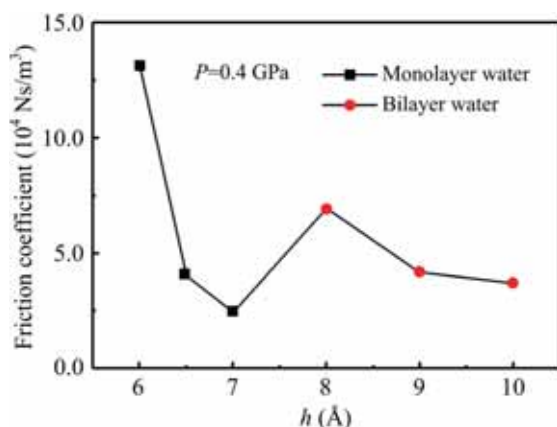


Fig. 5 Friction coefficient of the confined water at the water/graphene interface as a function of the nanochannel height h under $P = 0.4 \text{ GPa}$.

According to this theory, the interfacial friction coefficient is directly correlated with static rms force $\langle F^2 \rangle$, which can be given as follows:^{23,25}

$$\frac{\langle F^2 \rangle}{A} \cong \frac{1}{2} \rho_1 [S_1(\mathbf{q}_+) + S_1(\mathbf{q}_-)] (q_0 \Delta E^2) \quad (2)$$

where ρ_1 is the area density of the water molecules in the first layer near to the graphene wall, S_1 is the structure factor of the first water layer, ΔE is the interfacial interaction energy barrier at the position of the first water layer, and \mathbf{q}_\pm is the reciprocal lattice vector of the graphene wall. $\mathbf{q}_\pm = q_0 (1/\sqrt{3}; \pm 1)$ with $q_0 = 2\pi/(\sqrt{3}a_{\text{CC}})$, where a_{CC} is the carbon–carbon bond length. In this study, the value of $|\mathbf{q}_\pm|$ is about 29.5 nm^{-1} .

According to eqn (2), there are mainly two terms affecting the friction coefficient: one is the water structural parameter $\rho_1 S_1$ and the other is the interfacial interaction energy barrier ΔE . Herein, the contributions of these two terms to the friction coefficient were evaluated. Fig. 6a presents the structure factors of the confined water under different pressures at $h = 7 \text{ \AA}$. The structure factor was calculated by the equation used in ref. 23 and 36. As shown in the figure, the structure factor of the confined water is apparently affected by the lateral pressure. The maximum value of the structure factor S_{max} increases with P . Moreover, note that the values of S_{max} are smaller than 2.85,³⁷

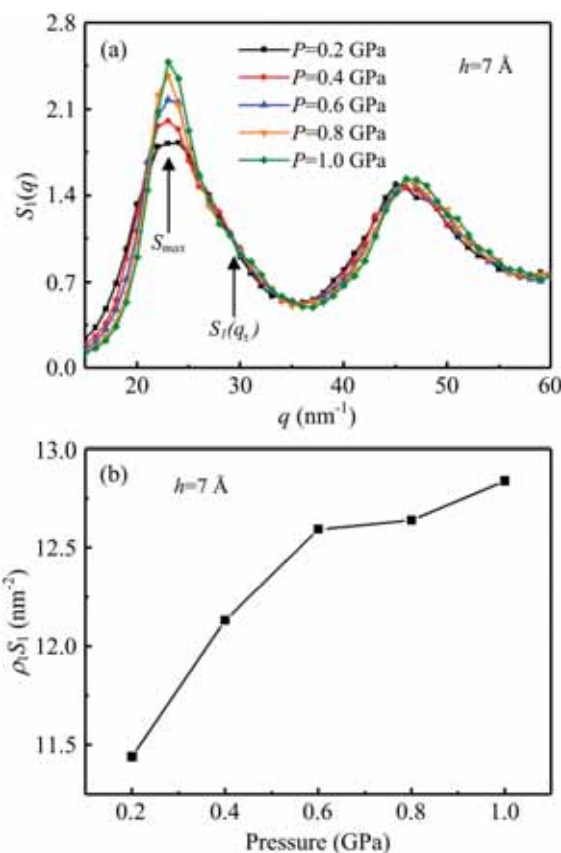


Fig. 6 (a) Structure factors, $S(q)$, of the water layer confined in the graphene nanochannel under different lateral pressures at $h = 7 \text{ \AA}$. (b) The structural parameter $\rho_1 S_1$ as a function of the lateral pressure at $h = 7 \text{ \AA}$.

indicating that the confined water is in the liquid phase when P is below 1 GPa. Fig. 6b illustrates the values of the structural parameter $\rho_1 S_1$ under different lateral pressures. The increasing trend of the structural parameter matches very well with the friction coefficient variation at $h = 7 \text{ \AA}$ (see Fig. 4), suggesting that this pressure-induced structure change of the trapped water is responsible for the pressure-dependent friction of the confined water.

Fig. 7(a) reveals the variation of the interfacial interaction energy barrier ΔE with respect to the distance from a single water molecule to the graphene surface (d_{w-g}). The inset plot provides the two-dimensional interaction energy map between a single water molecule and the graphene surface at $d_{w-g} = 3 \text{ \AA}$. The interaction energy map was computed by scanning a single water molecule at different positions (x, y) in the plane ($z = d_{w-g}$) on top of the graphene surface ($z = 0$). ΔE is defined as the difference between the maximum and minimum interaction energy in the map. It can be observed that ΔE is strongly related to the water-graphene distance. In our model, when the nanochannel height changes, the distance from the water layer to the graphene wall would consequently change, leading to the large variation of ΔE . Moreover, according to eqn (2), ΔE has a quadratic relation with the rms force. Therefore, it was

inferred that the dependence of friction on h was mainly caused by the variation of ΔE . To prove this, we calculated the average water-graphene distance \bar{d}_{w-g} from the water molecules in the first water layer to the graphene wall at different confinement heights. The upper plot in Fig. 7(b) presents the calculated \bar{d}_{w-g} as a function of the nanochannel height. \bar{d}_{w-g} shows an obvious variation as the h increases. Then, using \bar{d}_{w-g} , we calculated the corresponding energy barrier $\bar{\Delta E}$ acting upon a single water molecule, as shown in the lower plot in Fig. 7(b). We found that the trend of $\bar{\Delta E}$ variation was almost the same as that of the friction coefficient (Fig. 5) at different nanochannel heights under $P = 0.4 \text{ GPa}$, supporting the abovementioned proposed mechanism.

Based on the abovementioned analyses, the physical origin of the dependence of the interfacial friction coefficient on the lateral pressure and nanochannel height was proposed. For the pressure dependence, the increase of the friction coefficient with P is mainly caused by the pressure-induced structure change of water inside the nanochannel. For the nanochannel height dependence, the variation of the friction coefficient with h is induced by variation of the interaction energy barrier.

4. Conclusions

In summary, molecular dynamics simulations of the pressure-driven water flow confined in a graphene nanochannel were performed to investigate the structure evolution and dynamics of the constrained water. Depending on the lateral pressure ($P \leq 4.1 \text{ GPa}$) and nanochannel height ($6 \text{ \AA} \leq h \leq 10 \text{ \AA}$), the confined water at room temperature was found to exhibit phase transitions from liquid to ice of different structure, including flat monolayer square-like ice, puckered monolayer square-like ice, AB-stacked bilayer ice, AA-stacked bilayer ice, and ABA-stacked trilayer ice. Then, the friction coefficient at the water/graphene interface was calculated. We found that the interfacial friction coefficient gradually increases with the lateral pressure in the range of 1 GPa, under which the confined water is still in the liquid state. In addition, the interfacial friction coefficient also shows a dependence on the nanochannel height. To clarify the physical mechanism of this dependence of friction, theoretical analyses were conducted based on the Green-Kubo relation. We found that the pressure-dependent friction coefficient was mainly caused by the pressure-induced water structure change and the confinement-dependent friction results from the variations in the interfacial interaction energy barrier at different nanochannel heights. Overall, this study extends our understanding of the dynamics of the nanoconfined water in the presence of pressure at the gigapascal level. The dependence of friction found in this study may have a crucial effect on the transport behavior of the nanoconfined water and should be carefully considered while designing nanofluidic devices.

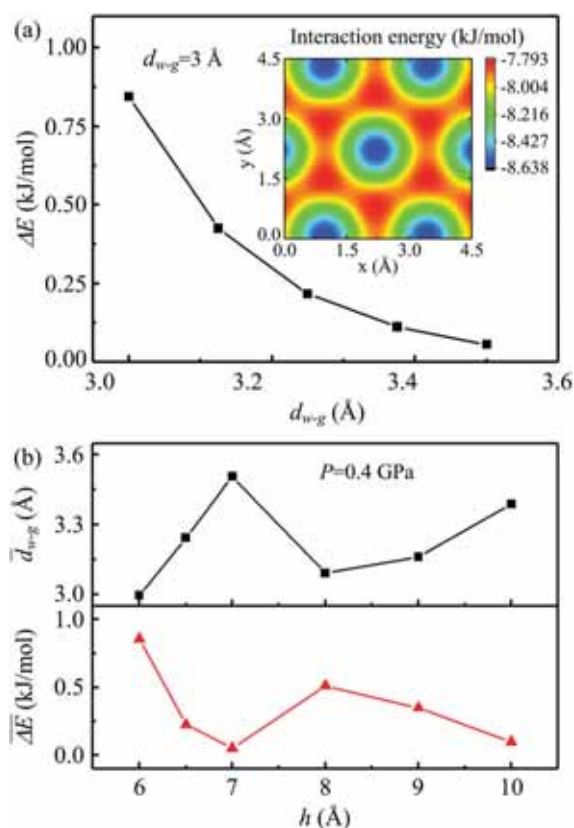


Fig. 7 (a) Interfacial interaction energy barrier ΔE as a function of the water-graphene distance d_{w-g} . The inset shows the interaction energy landscape felt by a single water molecule at a water-graphene distance of 3 \AA . (b) The average water-graphene distance \bar{d}_{w-g} and the corresponding energy barrier $\bar{\Delta E}$ as a function of the nanochannel height h under $P = 0.4 \text{ GPa}$.

Acknowledgements

The authors thank the National Natural Science Foundation of China under Grant No. 51605369 and 51575359, China

Postdoctoral Science Foundation under Grant No. 2015M572547. This work was also supported by HPC Platform, Xi'an Jiaotong University.

References

- H. Y. Yang, Z. J. Han, S. F. Yu, K. L. Pey, K. Ostrikov and R. Karnik, *Nat. Commun.*, 2013, **4**, 2220.
- Y. Kong, X. Fan, M. H. Zhang, X. Hou, Z. Y. Liu, J. Zhai and L. Jiang, *ACS Appl. Mater. Interfaces*, 2013, **5**, 7931–7936.
- S. X. Li, W. H. Guan, B. Weiner and M. A. Reed, *Nano Lett.*, 2015, **15**, 5046–5051.
- J. Y. Su and H. X. Guo, *J. Phys. Chem. B*, 2012, **116**, 5925–5932.
- S. Karan, S. Samitsu, X. S. Peng, K. Kurashima and I. Ichinose, *Science*, 2012, **335**, 444–447.
- J. Song, Q. Li, X. F. Wang, J. Y. Li, S. Zhang, J. Kjems, F. Besenbacher and M. D. Dong, *Nat. Commun.*, 2014, **5**, 4837.
- N. Raghav, S. Chakraborty and P. K. Maiti, *Phys. Chem. Chem. Phys.*, 2015, **17**, 20557–20562.
- Q. Li, J. Song, F. Besenbacher and M. D. Dong, *Acc. Chem. Res.*, 2015, **48**, 119–127.
- H. B. Huang, Z. G. Song, N. Wei, L. Shi, Y. Y. Mao, Y. L. Ying, L. W. Sun, Z. P. Xu and X. S. Peng, *Nat. Commun.*, 2013, **4**, 2979.
- M. Thomas, B. Corry and T. A. Hilder, *Small*, 2014, **10**, 1453–1465.
- N. Wei, X. S. Peng and Z. P. Xu, *Phys. Rev. E: Stat., Nonlinear, Soft Matter Phys.*, 2014, **89**, 012113.
- S. McKenzie and H. C. Kang, *Phys. Chem. Chem. Phys.*, 2014, **16**, 26004–26015.
- M. Ghosh, L. Pradiptanti, V. Rai, D. K. Satapathy, P. Vayalamkuzhi and M. Jaiswal, *Appl. Phys. Lett.*, 2015, **106**, 241902.
- B. Liu, R. B. Wu, J. A. Baimova, H. Wu, A. W. K. Law, S. V. Dmitriev and K. Zhou, *Phys. Chem. Chem. Phys.*, 2016, **18**, 1886–1896.
- R. R. Nair, H. A. Wu, P. N. Jayaram, I. V. Grigorieva and A. K. Geim, *Science*, 2012, **335**, 442–444.
- K. S. Vasu, E. Prestat, J. Abraham, J. Dix, R. J. Kashtiban, J. Beheshtian, J. Sloan, P. Carbone, M. Neek-Amal, S. J. Haigh, A. K. Geim and R. R. Nair, *Nat. Commun.*, 2016, **7**, 12168.
- J. I. Bai and X. C. Zeng, *Proc. Natl. Acad. Sci. U. S. A.*, 2012, **109**, 21240–21245.
- Y. B. Zhu, F. C. Wang, J. I. Bai, X. C. Zeng and H. A. Wu, *ACS Nano*, 2015, **9**, 12197–12204.
- J. Chen, G. Schusteritsch, C. J. Pickard, C. G. Salzmann and A. Michaelides, *Phys. Rev. Lett.*, 2016, **116**, 025501.
- G. Algara-Siller, O. Lehtinen, F. C. Wang, R. R. Nair, U. Kaiser, H. A. Wu, A. K. Geim and I. V. Grigorieva, *Nature*, 2015, **519**, 443–445.
- L. Bocquet and E. Charlaix, *Chem. Soc. Rev.*, 2010, **39**, 1073–1095.
- S. K. Kannam, B. D. Todd, J. S. Hansen and P. J. Daivis, *J. Chem. Phys.*, 2012, **136**, 024705.
- K. Falk, F. Sedlmeier, L. Joly, R. R. Netz and L. Bocquet, *Nano Lett.*, 2010, **10**, 4067–4073.
- G. Tocci, L. Joly and A. Michaelides, *Nano Lett.*, 2014, **14**, 6872–6877.
- W. Xiong, J. Z. Liu, M. Ma, Z. P. Xu, J. Sheridan and Q. S. Zheng, *Phys. Rev. E: Stat., Nonlinear, Soft Matter Phys.*, 2011, **84**, 056329.
- J. L. F. Abascal and C. Vega, *J. Chem. Phys.*, 2005, **123**, 234505.
- C. Vega, E. Sanz and J. L. F. Abascal, *J. Chem. Phys.*, 2005, **122**, 114507.
- T. Werder, J. H. Walther, R. L. Jaffe, T. Halicioglu and P. Koumoutsakos, *J. Phys. Chem. B*, 2003, **107**, 1345–1352.
- L. W. Li, D. Bedrov and G. D. Smith, *J. Phys. Chem. B*, 2006, **110**, 10509–10513.
- J. A. Thomas, R. M. Iutzi and A. J. H. McGaughey, *Phys. Rev. B: Condens. Matter Mater. Phys.*, 2010, **81**, 045413.
- Y. B. Wu and N. R. Aluru, *J. Phys. Chem. B*, 2013, **117**, 8802–8813.
- S. Plimpton, *J. Comput. Phys.*, 1995, **117**, 1–19.
- L. Bocquet and J. L. Barrat, *Soft Matter*, 2007, **3**, 685–693.
- P. Espanol and I. Zuniga, *J. Chem. Phys.*, 1993, **98**, 574–580.
- W. H. Zhao, J. Bai, L. F. Yuan, J. Yang and X. C. Zeng, *Chem. Sci.*, 2014, **5**, 1757–1764.
- J. L. Barrat and L. Bocquet, *Faraday Discuss.*, 1999, **112**, 119–127.
- J. P. Hansen and L. Verlet, *Phys. Rev.*, 1969, **184**, 151–161.